NASA/TM—1999–209481

The Geomagnetic Field and Radiation in Near-Earth Orbits

J.R. Heirtzler, Goddard Space Flight Center, Greenbelt, MD

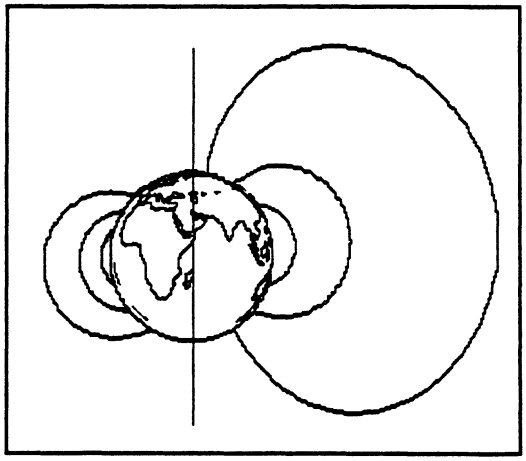

Geomagnetic Field Lines
From 40 W and 140 E

National Aeronautics and
Space Administration

Goddard Space Flight Center
Greenbelt, Maryland 20771

October 1999

The NASA STI Program Office ... in Profile

Since its founding, NASA has been dedicated to the advancement of aeronautics and space science. The NASA Scientific and Technical Information (STI) Program Office plays a key part in helping NASA maintain this important role.

The NASA STI Program Office is operated by Langley Research Center, the lead center for NASA's scientific and technical information. The NASA STI Program Office provides access to the NASA STI Database, the largest collection of aeronautical and space science STI in the world. The Program Office is also NASA's institutional mechanism for disseminating the results of its research and development activities. These results are published by NASA in the NASA STI Report Series, which includes the following report types:

- TECHNICAL PUBLICATION. Reports of completed research or a major significant phase of research that present the results of NASA programs and include extensive data or theoretical analysis. Includes compilations of significant scientific and technical data and information deemed to be of continuing reference value. NASA's counterpart of peer-reviewed formal professional papers but has less stringent limitations on manuscript length and extent of graphic presentations.
- TECHNICAL MEMORANDUM. Scientific and technical findings that are preliminary or of specialized interest, e.g., quick release reports, working papers, and bibliographies that contain minimal annotation. Does not contain extensive analysis.
- CONTRACTOR REPORT. Scientific and technical findings by NASA-sponsored contractors and grantees.
- CONFERENCE PUBLICATION. Collected papers from scientific and technical conferences, symposia, seminars, or other meetings sponsored or cosponsored by NASA.
- SPECIAL PUBLICATION. Scientific, technical, or historical information from NASA programs, projects, and mission, often concerned with subjects having substantial public interest.
- TECHNICAL TRANSLATION. English-language translations of foreign scientific and technical material pertinent to NASA's mission.

Specialized services that complement the STI Program Office's diverse offerings include creating custom thesauri, building customized databases, organizing and publishing research results ... even providing videos.

For more information about the NASA STI Program Office, see the following:

- Access the NASA STI Program Home Page at http://www.sti.nasa.gov/STI-homepage.html
- E-mail your question via the Internet to help@sti.nasa.gov
- Fax your question to the NASA Access Help Desk at (301) 621-0134
- Telephone the NASA Access Help Desk at (301) 621-0390
- Write to:
  NASA Access Help Desk
  NASA Center for AeroSpace Information
  7121 Standard Drive
  Hanover, MD 21076-1320

NASA/TM—1999–209481

The Geomagnetic Field and Radiation in Near-Earth Orbit

J.R. Heirtzler, Goddard Space Flight Center, Greenbelt, MD

National Aeronautics and
Space Administration

Goddard Space Flight Center
Greenbelt, Maryland 20771

October 1999

Acknowledgments

The author appreciates comments made by S. Fung, D. Stern, and M. Purucker, on a draft of this report, although the author is solely responsible for its content.

Available from:

NASA Center for AeroSpace Information
7121 Standard Drive
Hanover, MD 21076-1320
Price Code: A17

National Technical Information Service
5285 Port Royal Road
Springfield, VA 22161
Price Code: A10

ABSTRACT

This report shows, in detail, how the geomagnetic field interacts with the particle flux of the radiation belts to create a hazard to spacecraft and humans in near-Earth orbit. It illustrates the geometry of the geomagnetic field lines, especially around the area where the field strength is anomalously low in the South Atlantic Ocean. It discusses how the field will probably change in the future and the consequences that may have on hazards in near space.

CONTENTS

FIGURES

TABLES

INTRODUCTION

It has been known for more than 40 years that the anomalously weak geomagnetic field in the South Atlantic Ocean, near the coast of Brazil, is important to the radiation environment near Earth. Radiation belt particles, trapped by lines of force of the geomagnetic field, approach closer to the Earth's surface here than elsewhere. This is an area of intense radiation in near-space and is a subject of extensive research by space scientists. This radiation is usually described on a heuristic basis from measurements made in space and "models" have been developed on this basis. There are also attempts to understand the radiation in terms of the laws of physics, i.e., particle motion in the geomagnetic field, and how to effect shielding from this radiation. Space mission and instrument designers today rely on both these approaches.

There is an increasing use of near-Earth orbits for spacecraft to study the Earth, for space telescopes, for the manned space station, and for military and commercial applications. All these spacecraft and humans in space suffer very significant damaging effects of radiation. Since most of this radiation is related to the geomagnetic field, this report will take a brief but closer look at the correspondence between the geomagnetic field and radiation and how this situation may become worse in the future.

Many studies of radiation in near space have treated the geomagnetic field as if it was due to a simple dipole. With the current field model we examine details of the field at any latitude, longitude, and altitude, out to about 4 Earth radii (25,484 km) where solar time-varying effects become important and the magnetospheric boundary is felt. Many features of the actual geomagnetic field in space have not been illustrated and this report attempts to show that.

The IGRF spherical harmonic coefficients for 1995 (Barton, C.E. et al.,1996) are used to represent the actual geomagnetic field, as of the beginning of the year 1995. This version of the IGRF, as of this writing, is the most recently approved reference field and has been extensively studied in many publications. This IGRF model also carries the time derivative of the spherical harmonic coefficients so one may calculate the time variations of the field (although one is cautioned that the accuracy will degenerate if the calculation is extended too far from 1995). The three-dimensional complexity of the geomagnetic field is such that one should have a computer to display any of the many aspects of the field geometry, or show how the degree and order of the IGRF terms influence the field configuration[1]. Here we used the IGRF to degree (n) and order (m) 10, although fewer terms were occasionally used to see how significantly they

---

[1]A desktop computer was used to calculate the geomagnetic field components from the International Geomagnetic Reference Field (IGRF) coefficients and to produce simple graphics. Computer codes for calculations and graphics were written in TrueBasic. A subroutine to calculate the field from the spherical harmonic coefficients follows that of Quinn (Quinn, et al., 1995) and sources quoted there, converted from the original Fortran to TrueBasic language (see appendix). These programs were run on a Power Macintosh 9600 desktop computer.

There are several programs available to calculate the field components from the IGRF coefficients, for example see http:// www.ngdc.noaa.gov/IAGA/wg8/wg8.html.

To make global maps of the geomagnetic field the total field was calculated for each 5 degrees of latitude and 5 degrees of longitude and compared to published tables of these values, where available. The results matched to within a few nT. This matrix of values was entered in a graphics program (Spyglass) and the results contoured to produce maps of the total field of the Earth.

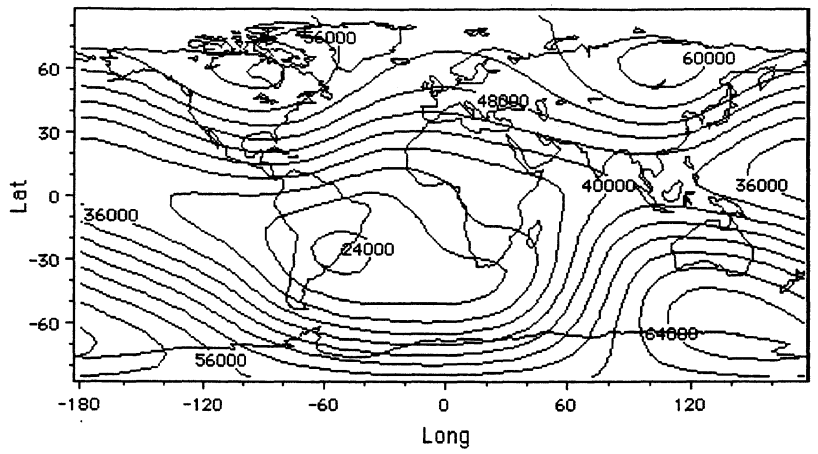

Figure 1. Contours of total field intensity, in nT, at the Earth's surface, using IGRF 95.

changed the results and to see how the field appears with only the tilted and displaced dipole. It is the total field magnitude, rather than field components, that are sufficient for purposes of this report; however, the directions of the field are used in the ray tracing of the lines of force.

Four principal anomalous regions of the field at the Earth's surface are the localized highs in northern Siberia, in northern Canada and near Antarctica south of Australia, and the large, elongated low near the coast of Brazil. This later feature is the South Atlantic Anomaly (SAA)[2], with a minimum of about 23,000 nT located at 26 S, 53 W, about 700 km inland from the coast of Brazil. It is frequently said that the SAA is due to the displacement of the geomagnetic dipole axis from the center of the Earth, in the direction of the Pacific Ocean and the tilt of the dipole with respect to the rotational axis.

This point is made clear in figure 2. The upper part of this figure shows the field that would result from an axial, inclined dipole. That is the field that is produced using only the first three terms of the IGRF 1995, all of which have n = 1. In equatorial latitudes the contours follow the magnetic equator.

The lower part of figure 2 shows the field that would be produced by an offset, inclined dipole. This field is due to only the first 8 terms of the IGRF 1995, where terms have n = 1 and 2. The displacement of the dipole is 526.89 km in the direction of the northwest Pacific (21.47 N, 144.77 E). The inclined, offset dipole creates an Antarctic high south of Australia and an SAA off Brazil but it does not create the highs in Northern Canada and Siberia. The SAA in this figure has many of the characteristics of the SAA of the complete field (figure 1). However, the actual SAA is stretched more towards the southern tip of Africa, showing that terms with n greater than 2 play a significant role shaping that Anomaly. The shape of the field contours in figure 2 (Lower) greatly resemble the actual field at an altitude of 5000 km (figure 3, lower right), showing that terms with n greater than 2 have little effect at this altitude.

---

[2]The SAA was also called the Brazilian Anomaly (Dessler and Karplus, 1960) or Capetown Anomaly (Heirtzler and Hirshman, 1960: Cain, et al., 1968).

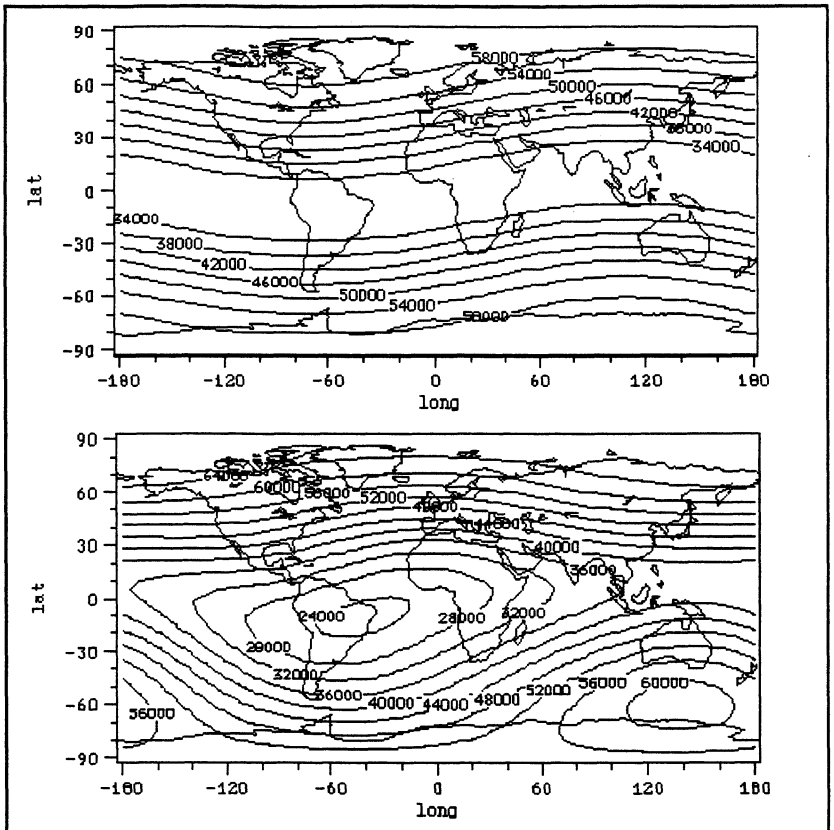

Figure 2. (Upper) Total Field (nT) due to centered, inclined dipole. (Lower) Total Field (nT) due to offset, inclined dipole.

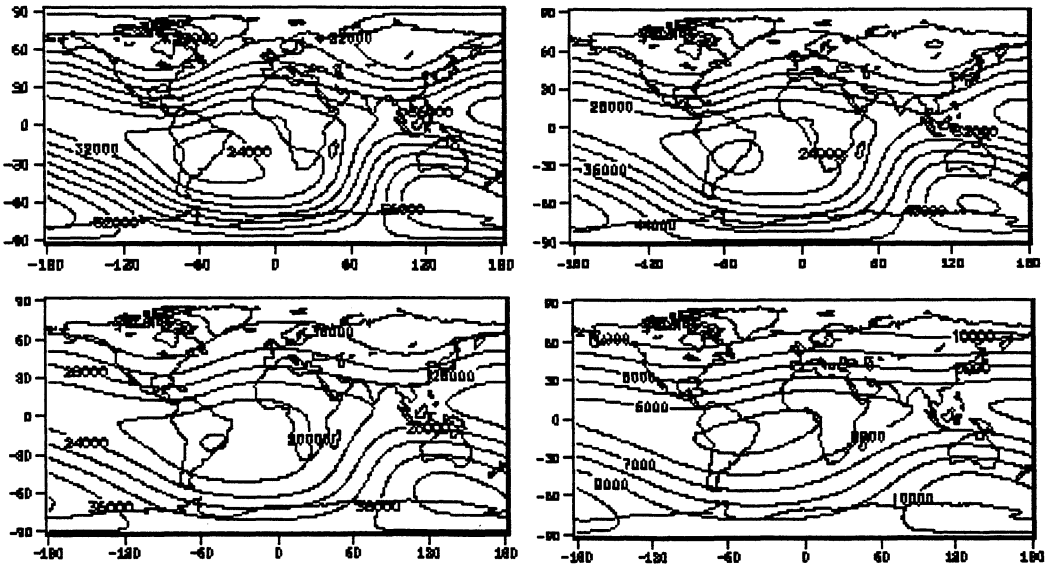

Figure 3. Contours of total field intensity, in nT, at various altitudes above the Earth's surface, using IGRF 95. Upper left 200 km altitude, upper right 500 km, lower left 1000 km, lower right 5000 km.

Maps of the total field at elevations of 200, 500, 1000, and 5000 km are shown in figure 3. Many low-Earth orbit (LEO) spacecraft fly at altitudes between 500 and 1000 km and the field they experience is shown here. The shape of the contours of the SAA are rather different than at the Earth's surface. The weakest part of the field is still off the coast of Brazil but there is a tendency for the low to be stretched in the direction of Africa. From 200 to 500 km the strength of the SAA is reduced by about 4000 nT, and from 500 to 1000 km the SAA is reduced by another 4000 nT. At 5000 km the overall field strength is much reduced over its value at lower elevations, rarely reaching 10,000 nT, and the difference between highs and lows is less pronounced.

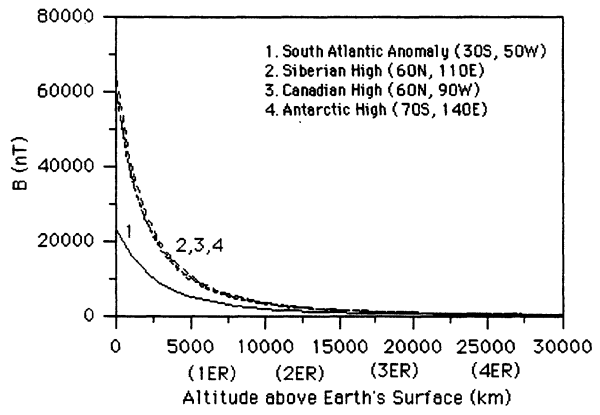

Figure 4. Field strength as function of altitude above four anomalous areas of the Earth's surface.

The variation of the field with altitude over the four anomalous regions is shown in figure 4. The SAA low covers a larger portion of the Earth's surface than the highs and figure 4 shows that the variation with height for the SAA is much less than for the other three areas. For all the regions the field strength at 5000 km is about one-third what it is on the surface. At 10,000 km (somewhat less than 2 Earth radii) the field strength is about one-tenth the surface value. Above about 15,000 km (not shown) the field strength is much reduced and the four anomalous regions (including the SAA) have lost their distinctive appearances. Geostationary orbits (36,000 km) are beyond the influence of the SAA, although there are other radiation hazards, due to other effects, at this altitude.

GEOMAGNETIC FIELD LINES IN SPACE

Usually early drawings of the Earth's magnetic field lines were more cartoon than fact and did not reflect their true configuration. However, there were attempts to describe the geomagnetic field in a fashion useful for studying the radiation environment (for example McIlwain, 1961; Mlodnosky and Helliwell, 1962). With the availability of inexpensive but fast desktop computers it is easy to get an accurate presentation of the field using all the spherical harmonic components. We show some examples here.

The straightforward procedure for drawing a line of force (ray tracing) is to start with a point at a given latitude, longitude and altitude. For this point the IGRF is used to find the direction of the field (declination and inclination). The next point will be a specified distance in the direction indicated by the field. The accuracy of the position of the line of force will depend upon this step size. The smaller the step size the more accurate the line but the longer it will take the program to run. Using different step sizes we found that a 110-km step produced sufficient accuracy, although this was slightly degraded along arcs at distances of about 4 Earth radii.

For this second point the direction of the field was again calculated, and position of the third position determined, etc., with the process stopping when the next altitude would be less than zero. This provides a series of points defining a line of force with the coordinates and field components specified for each point. Usually we took lines originating in the Southern Hemisphere (because the SAA is in the Southern Hemisphere) with a loop stepping the origin to different starting latitudes and/or longitudes as each line is finished. In special cases, for example, where we are plotting lines crossing the shuttle's path (figure 7), it was necessary to start the line on the shuttle's path and proceed in both south and north directions from there.

To illustrate the asymmetry of the lines of force we show (figure 5) lines of force originating along 40 W near the longitude of the SAA and also along 140 E, which is separated by 180 degrees and is near the longitude of the Antarctic and Siberian highs. Here the lines originate at 20, 40, and 60 S. Lines which originate at 60 S reach nearly 4 ER near the equator along 140 E but only about 1 ER on the opposite side of the Earth. Notice that the line which leaves 60 S terminates near 80 N along 140 E, but only at about 45 N along 40 E. The tilt of the dipole axis is evident. When the Earth rotates during the course of the day, this asymmetric field creates a changing, magnetically complex region in near space.

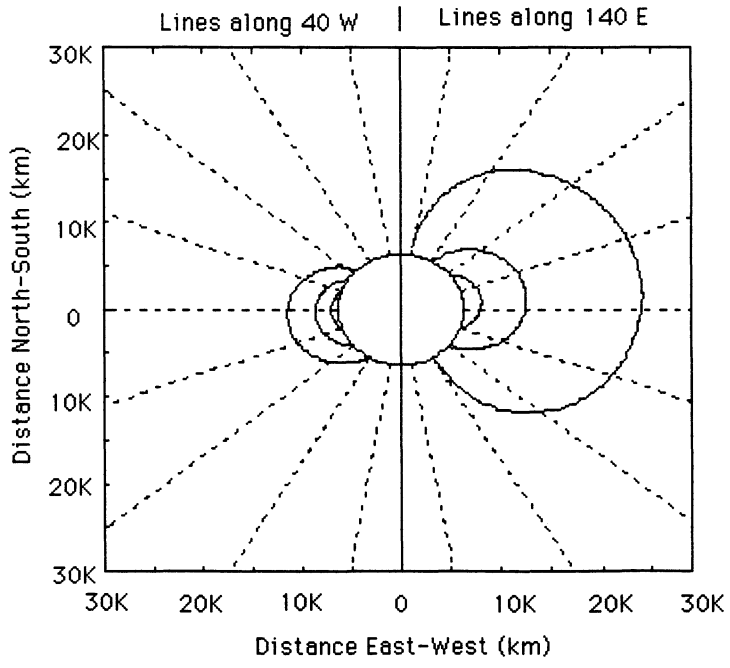

Figure 5. Lines of force from opposite sides of the Earth. Lines originate from 20 S, 40 S, and 60 S, and from 40 W (near the SAA) and 140 E (near the Siberian and Antarctic highs).

Figure 6 is another display of field lines, originating at various longitudes but always from 70 S. This displays the range of altitudes reached by lines originating from different longitudes. For this latitude (70 S) lines starting from 80 W are closest to the surface of the Earth and the line staring from 120 E are the most distant. It is clear that any charged particle within 1 or 2 ER would experience different forces depending upon which side of the Earth it approached.

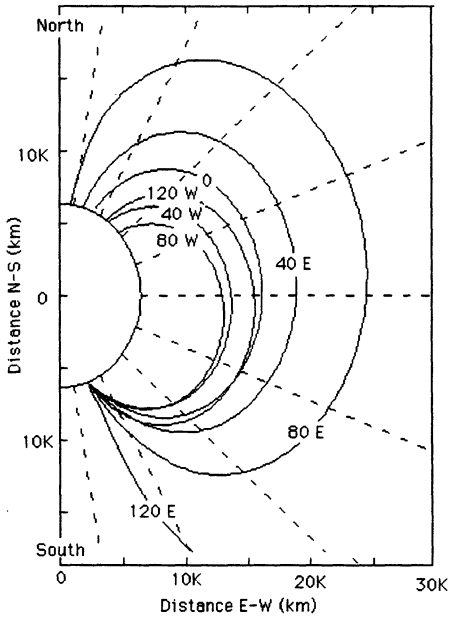

Figure 6. Lines of force from 70 S, for various longitudes.

Another way of getting a broad view of field lines is to show their projection on the surface of the Earth (figure 7). Here lines originate at 10, 30, and 50 S and at various longitudes. The projection of the line which originates near the SAA (30 S, 30 W) appears to cross the line originating at 50 S, 30W. Other lines appear to cross as well.

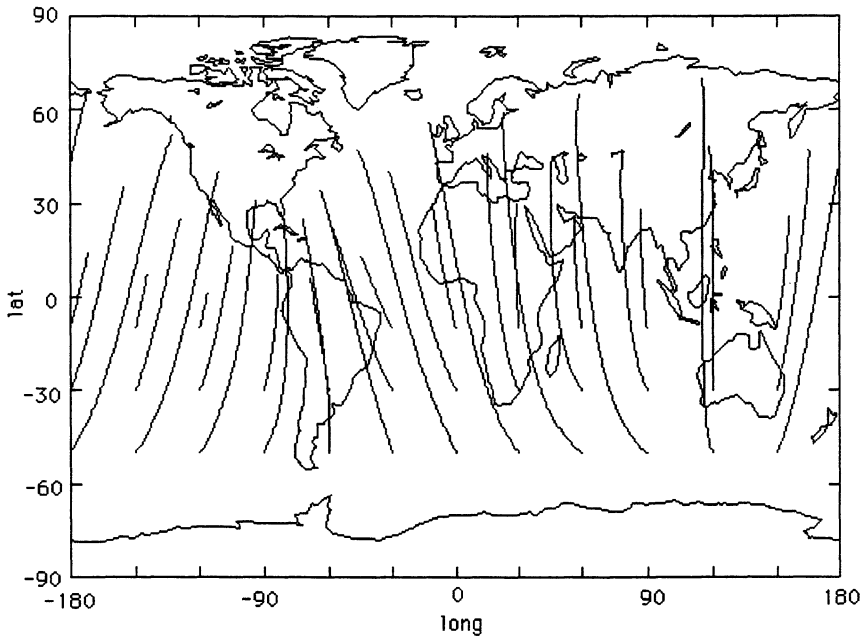

Figure 7. Lines of force originating from 10 S, 30 S, and 50 S, and from each 30 degrees of longitude, as projected on the Earth's surface.

Actually they are at different altitudes and do not physically cross in space. If one looks at the lines of force crossing the shuttle's path one gets another perspective (figure 8). Since the shuttle is at constant altitude (480 km here) it will cross more polar or more equatorial lines as it moves from high to low latitudes. These are shown for two common orbital inclinations: 28.5 and 57 degrees. In both cases an orbit was chosen which goes through the SAA. On the 28.5 degree inclination orbit none of the lines of force reach high (auroral) latitudes. With the 57 degree orbit the shuttle is frequently near the ends of a line of force. In those higher latitudes the lines of force are nearly vertical and do not extend much past the flight path. At the equator the shuttle is near the top (maximum altitude) of the line of force and the lines of force are more horizontal.

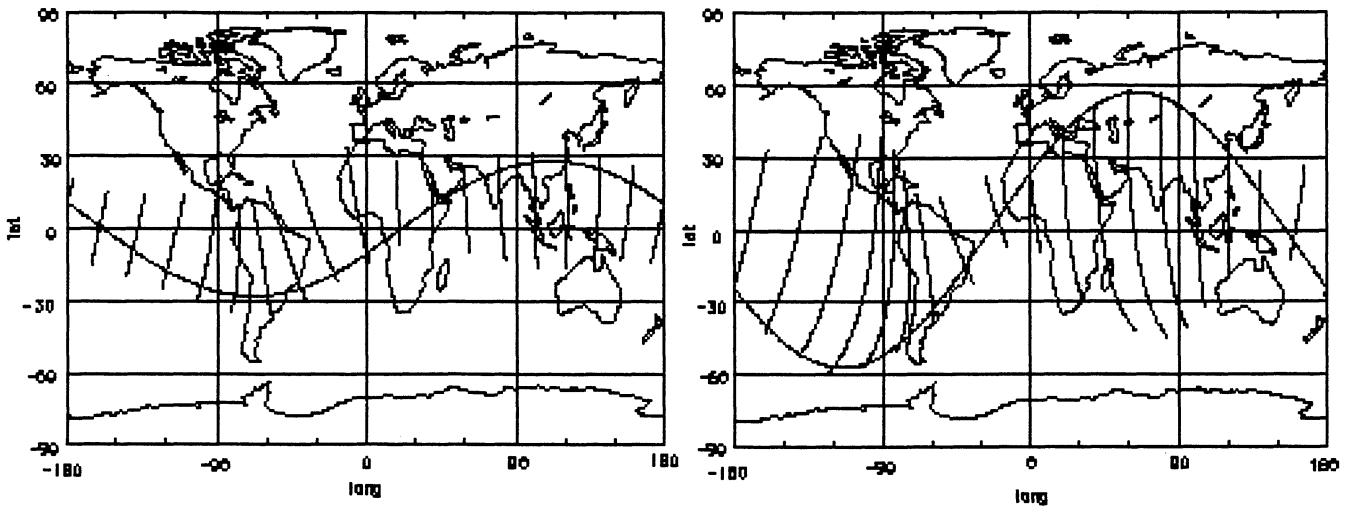

Figure 8. Lines of force crossed by the shuttle on an orbit crossing the SAA. On the left is an orbit with 28.5 degrees inclination. On the right is an orbit with 57m degrees inclination.

Figure 9 is yet another illustration of the lines near the SAA. It shows the field strength along three lines of force starting at latitudes 20 S, 30 S, and 40 S, all along 60 W and along three lines originating at 0, 30 W, and 60 W and all at 30 S. The further south the origin, the weaker the field near the equator because of its higher altitude, but the field is stronger at the ends of the lines where the lines are at higher latitudes. The field strength at the equator of the line starting on the Greenwich meridian is less than the others because that line rises to higher altitudes along the equator. One notices that all lines have the same strength at about 28 S, very near the latitude of the SAA. Of course, this does not mean that all lines have the same altitude at the crossover point shown.

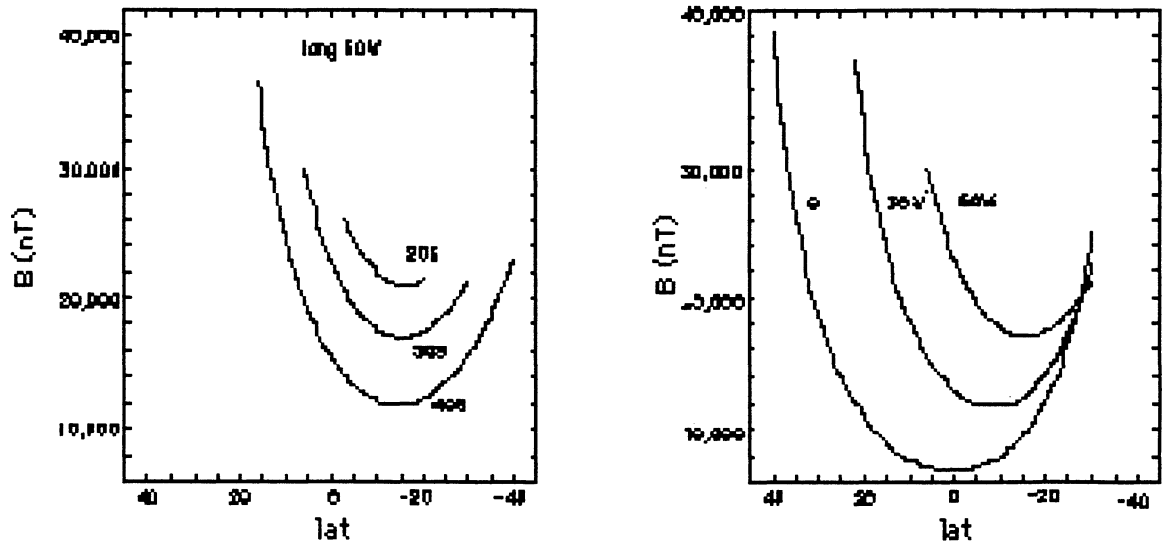

Figure 9. (Left) Field strength vs latitude for starting latitudes 20 S, 30 S, and 40 S, all at 60 W longitude. (Right) Field strength vs latitude for starting longitudes 0, 30 W, and 60 W.

PARTICLE MOTIONS AND THE UPPER ATMOSPHERE

For human safety and for engineering purposes it is important to know the radiation environment expected in near-space missions. Ad hoc "models" have been developed from observational data. There are two models. One model describes the electron flux and another the proton flux. NASA Trapped Radiation Models AE-8 and AP-8, for electron- and proton-produced radiation respectively, are available from the National Space Science Data Center (http://nssdc.gsfc.nasa.gov) and described by Fung, 1996. Countries other than the U.S., notably Britain and Russia, have other models. The models give the particle flux as a function of particle type, particle energy, position, and time.

No extensive discussion of charged particles in space will be given here, only enough of the basic principles to understand the effect of the geomagnetic field on the radiation. A more complete and convenient description can be found on the homepage of the (Belgium) Space Environment Information System (http://www.spenvis.oma.be/spenvis/)

The motion of a charged particle is characterized by the particle's energy, mass, charge and pitch angle at the equator (angle made with the line of force). Their motion in the radiation belts is depicted as being of three basic types, all occurring simultaneously and all controlled by the geomagnetic field (for general discussions see Walt, 1994, or Roederer, 1970). The first type of motion is a circular motion with a gyroradius about the field line (period of the order of milliseconds). This radius depends upon the strength of the field where the particle is located and its local pitch angle. Stronger fields cause the radius to be less; the radius is greater for greater pitch angles and greater energies. Figure 10 shows the radius for selected points, selected field lines, and selected energies for electrons and protons. It is seen that these radii are of the order of meters for electrons and kilometer for protons. The radius will change as the particle moves along a field line into different field strengths.

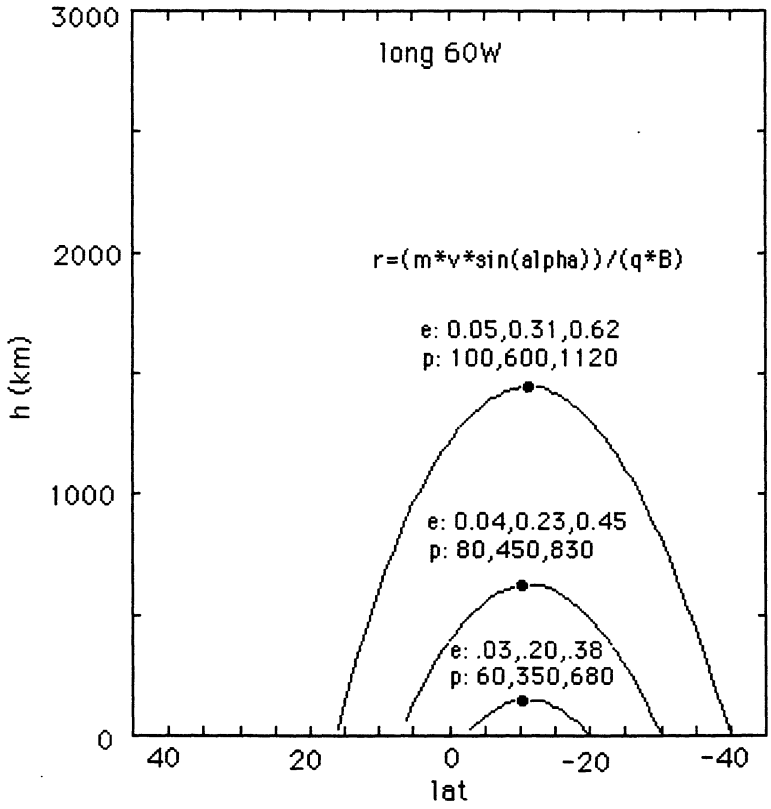

Figure 10. Heights of lines of force starting at 20 S, 30 S, and 40 S, all along longitude 60 W. The gyroradius for electrons (e), and protons (p), are given in meters for 1, 10, and 20 Mev particles at the equator with pitch angles of 90 degrees.

The second motion is the bounce back and forth along a field line from one hemisphere to the other, reversing direction at a mirror point. This period is on the order of seconds. This motion is an adiabatic invariant, requiring that the magnetic field strength divided by the square of the sine of the pitch angle is a constant anywhere along the field line, regardless of the charge, mass, or energy of the particle. Since the pitch angle at the mirror point (Φ_m) is 90 degrees we can find the value of the field strength at the mirror

point (B_m) by the equation

$$B_e / \sin^2(\Phi_e) = B_m / \sin^2(\Phi_m) = B_m \qquad (1)$$

where B_e is the field strength at the equator and Φ_e is the pitch angle at the equator and Φ_m is the pitch angle at the mirror point (90 degrees).

Since we know the angles of the field along the field line we can find the place where the dip angle changes sign, i.e., the equator, and the value of B_e there. Equation 1 shows that there is a different value of B_m for each equatorial pitch angle. Knowing B_m we can find the altitude of the mirror point. Figure 11 shows the heights of lines of force vs latitude for south points of origin along longitude 53 W. Only the lower 1000 km of these lines are shown and mirror altitudes are shown along each line for various equatorial pitch angles. Although the longitude of these lines goes through the SAA, this figure does not give any indication why charged particles are trapped at the SAA. The longer (higher altitude) field lines have lower pitch angles near the Earth's surface.

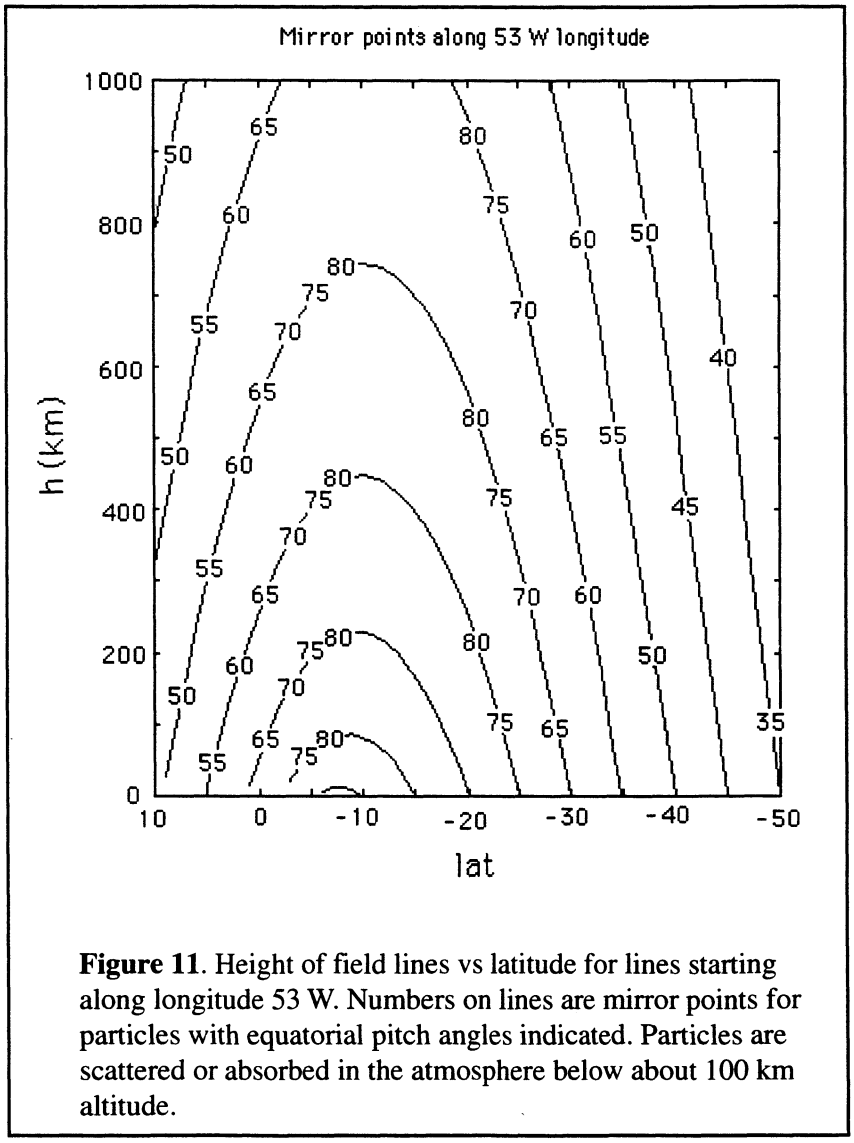

Figure 11. Height of field lines vs latitude for lines starting along longitude 53 W. Numbers on lines are mirror points for particles with equatorial pitch angles indicated. Particles are scattered or absorbed in the atmosphere below about 100 km altitude.

It should be kept in mind that the particle flux density is not the same for all angles at the equator. Here one relies on the cumulative observations that have been made on many spacecraft. The distribution of particle flux at the equator is expressed as function of pitch (Φ) angle by the expression

$$J(\Phi) = J \sin^{n} (\Phi) \tag{2}$$

Where J is a constant (value of $J(\Phi)$ when Φ=90) and n is the anisotropy index and has been given by Fung, 1996. Figure 12 is a plot of $\sin^{n} (\Phi)$, or the ratio of $J(\Phi)/J$, vs Φ for values of n from 1 to 8, indicating that, even for relatively small values of n, most of the flux will be at very high pitch angles.

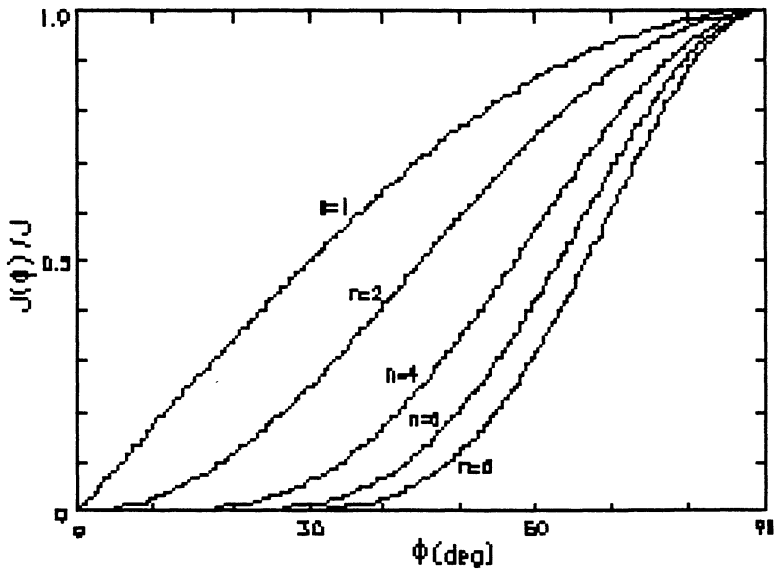

Figure 12. Normalized particle flux as function of pitch angle and anisotropy index n, at equator.

Fung shows the electron and proton particle density of a function of n, but the number of particles with lower values of n is relatively small. Then, referring to figure 11 we see that most particles have a mirror location in the upper part of their field lines and much fewer come to lower elevations where they might interact with the atmosphere.

The third type of motion is the drift of particles around the Earth from east to west or west to east, usually taking about an hour. As particles gyrate about a field line they reach neighboring field lines to the east or west. There may be a stronger or weaker field on the neighboring line, shortening or lengthening the gyroradius. This will cause the particle to drift to the east (electrons) or west (protons). This effect may be different at different altitudes, latitudes, and longitudes because the field strength varies with these variables. This motion of charged particles is called the "ring current."

Scattering by the atmosphere removes particles from the lower end of the radiation belts. This is illustrated by the reduction in astronauts' dose rate during sunspot maximum, compared to sunspot minimum (Badhwar, et al., 1997). At sunspot maximum the atmosphere is believed to expand due to heating, removing more particles from the lower end of the radiation belts. Although there are more solar flares—producing more particles in the radiation belts—during solar max, this effect is of shorter duration and is counter to the effect of removing radiation-belt particles by the expanded atmosphere.

Models of the upper atmosphere are available on-line from the National Space Science Data Center (NSSDC) at URL (http://nssdc.gsfc.nasa.gov/space/model/atmos/msice.html). This source provides data for the MSIS-E-90 (Mass-Spectrometer-Incoherent-Scatter) model, which in turn is based largely on the COSPAR International Reference Atmosphere (CIRA) 1986 model. This model is an improvement over the frequently quoted U.S. Standard Atmosphere (1976). Figure 13 shows, as an example, a height-density profile of the atmosphere for 06 hrs UT, 1 January 1995, in the vicinity of the SAA.

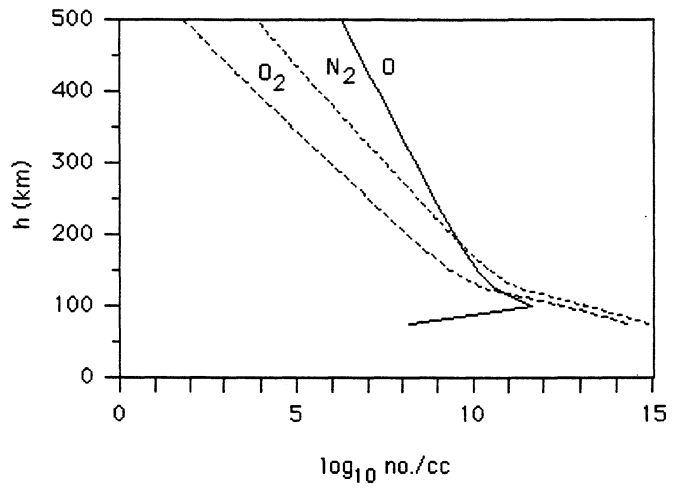

Figure 13. Number density profile with height for atomic oxygen (O), molecular nitrogen (N_2), and molecular oxygen (O_2).

On a worldwide basis the atmospheric density is highest in October and April and lower in July and January. It also varies with latitude, longitude, time of day, geomagnetic activity and, as just mentioned, sunspot cycle. NSSDC atmospheric models, plotted for different locations and times, show that most of the density change occurs in the lower atmosphere and that figure 13 is a typical example.

The number density is dominated by molecular nitrogen below 80 to 100 km. Above this altitude atomic oxygen dominates the particle number density. However, the total particle density (O plus N_2) drops off drastically by about 7 orders of magnitude. The sensible top of the atmosphere is usually taken to be 100 km.

Interactions with the atmosphere are not necessarily responsible for the increase in radiation over the SAA. However, the atmosphere is responsible for removing particles from the radiation belts.

RADIATION DAMAGE TO SPACECRAFT

There are many types of hazards to spacecraft. Aside from the hazards caused by space debris and the problems associated with the vacuum of space, there are effects caused by the interaction of spacecraft with its plasma environment. These include spacecraft wake effects, spacecraft contamination effects, spacecraft power system effects, and spacecraft electromagnetic effects. There are major effects due to the natural, undisturbed radiation in space and these we explore here.

All spacecraft suffer radiation damage. Designing electronics and other equipment to minimize the effect of this damage is a major engineering concern, affecting both the choice and redundance of electronic components and circuits, as well as software design. Especially over the SAA, there is significant radiation damage to electronic, optical, and computer systems. This radiation is of various types, depending upon the type of particle and its energy, the amount of radiation shielding, and the sensitivity of the materials receiving this radiation. One common type of radiation damage is spacecraft charging whereby charge is built up with time until arcing occurs. Another and very common type of damage is a "Single Event Upset" or SEU, whereby a single and critical digital component changes state. Clever design can frequently cause such problems to be reduced, although the spacecraft may be inoperative for a period of time. Some spacecraft turn off electrical circuits or optical systems when passing over the SAA.

Most ground controllers keep records of the type of damage, the time and where such damage occurred. An archive of such records is available from the National Geophysical Data Center in Boulder, URL address (http://spider.ngdc.noaa.gov:800/production/html/GOES/anom5jt.txt) or by ftp :// ftp.ngdc.noaa.gov/lSTP/ANOMALIES/.

An example of the SEU's for one spacecraft is given in figure 14. This is for TOPEX, at an altitude of 1340 km, for the period 1992–1998, with total field strength contours shown for approximately the same altitude. The points do not cluster evenly within a contour but are more scattered in a northeast-southwest direction. (Characteristically, SEU's for various spacecraft are not rigidly confined by any total field contour line.)

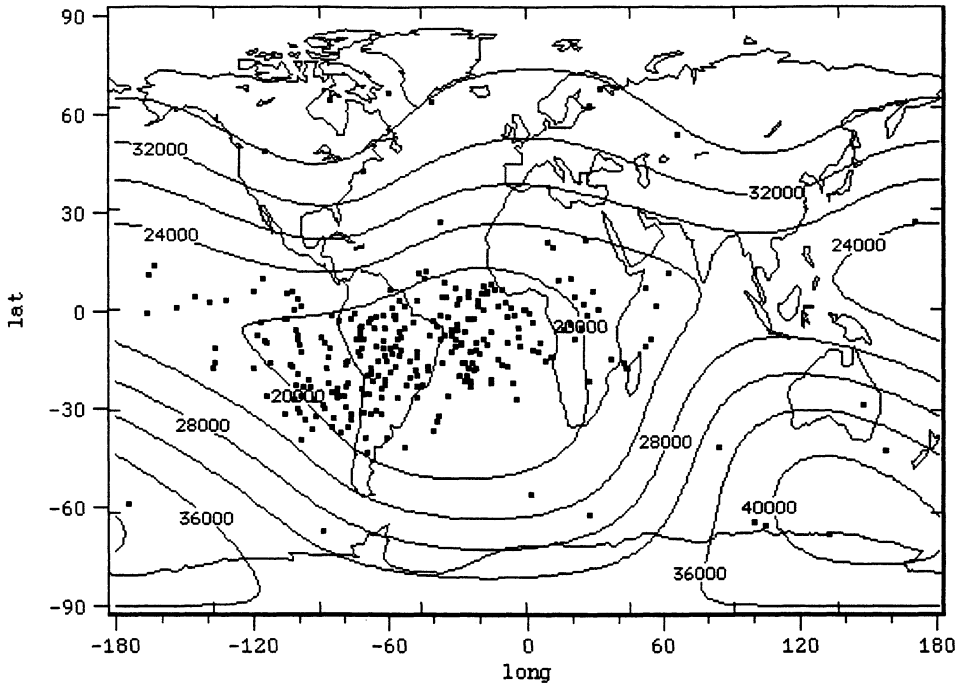

Figure 14. Location of Sudden Event Upsets (SEU's) for TOPEX for the years 1992–1998 with contours of total field intensity at 1000 km altitude for 1995.

There were 282 SEU's over this 6-year period. This rate of a few per week to a few per month seems typical. It is seen that most of the SEU's are located in and about the SAA, although there is no clear contour that defines where they will occur. An examination was made of South America geomagnetic observatory records for times when there was an SEU nearby. These records indicated no unusual geomagnetic activity. Another investigation looked at the 3-hour Ap activity index when there was an SEU. Figure 15 shows the distribution of Ap when there was an SEU. There are relatively few high Ap and the distribution of Ap is not greatly different from the distribution of all Ap during the 1992–1998 period. Although it is known that there is a burst of radiation in space when there are solar flares it is impossible to predict exactly when an SEU will occur. Table 1 is a list of some spacecraft which have been, are, or will be, in Low-Earth Orbit and suffer radiation damage. A notable case is the Hubble Space Telescope,

whose instruments are turned off over the SAA to prevent damage to its optical fibers, electronic components, and solar arrays. Other spacecraft have had problems with star cameras and other instruments. The shuttle, Mir, and the International Space Station Alpha are manned space missions which have operated or will operate for extended periods of time in this environment. Spacecraft in higher orbits also suffer radiation damage. For example, spacecraft in geosynchronous orbits, although at an altitude of 35,790 km (about 6 Earth radii) and in an equatorial orbit also suffer radiation damage. These spacecraft rotate with the line of force on which they are located and these lines terminate at very high latitudes on the Earth's surface.

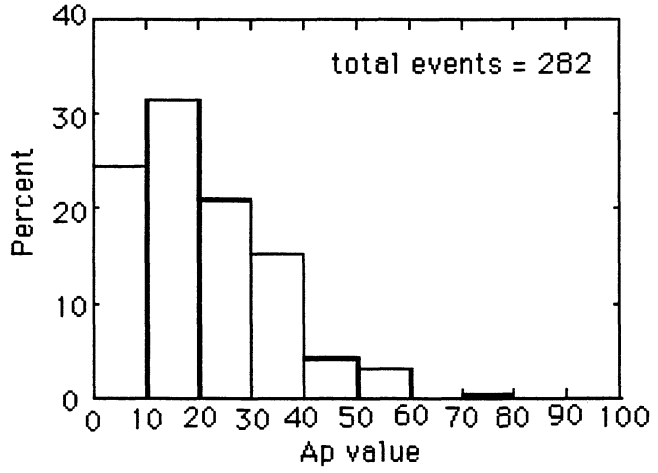

Figure 15. Distribution of Ap-index values for times of TOPEX SEU's.

Table 1. Some LEO Spacecraft.

Name	Country	Launch Date	Incl. (deg.)	Mean Alt. (km)
EXISTING				
ASTRID-2	SWEDEN	12/98	83	1000
COBE	US	11/89	99	882
ERS-1	ESA	7/91	99	784
EUVE	US	7/92	28	506
GRO	US	4/91	28	434
HST	US	4/90	28	595
LANDSAT-5	US	4/84	98	703
LANDSAT-7	US	4/99	98	700
MIR	RUSSIA	2/86	52	392
NOAA-12	US	5/90	99	815
OERSTED	DEN.	2/99	97	715
ROSAT	GER.	6/90	53	544
SAMPEX	US	7/92	82	593
SEAWTFS	US	9/97	98	705
SHUTTLE	US	many	28.5, 57	300
SPOT	FRANCE	several	99	825
SUNSAT	S. Afr.	2/99	96	715
TOPEX	US/FR	6/92	66	1338
TRIMM	US	11/97	35	350
UARS	US	8/91	57	578
PLANNED				
CHAMP	GER.	/00	85	375
DMSP-B5	US	8/99	polar	840
FEDSAT	AUST.	/01	70	750
GRADSAT	DEN.	/02	polar	600
NPOESS	US	/08	polar	833
SAC-C	ARGEN.	12/ 99	98	702
SAC1-1	BRAZIL	7/99	99	750
VCL	US	2/00	65	400
GLAS	US	/01	94	600

RADIATION HAZARDS TO HUMANS

Radiation in the radiation belts offer several constraints and hazards to humans in low-Earth orbit. The ionizing radiation found in LEO is thought to come, largely, from two sources: (1) trapped radiation which originates on the Sun and with the proton component being the most dangerous, and (2) galactic cosmic rays, which are extremely energetic and which occur at unpredictable times. Shielding offers little protection from radiation belt particles from the Sun and virtually no protection from galactic rays (see Wilson, et al., 1997). Outside the Earth's magnetic field (outside the magnetosphere) there are other very significant radiation hazards but, since those are not controlled by the Earth's magnetic field, they will not be discussed here. The environment of low-Earth orbit is where humans will be spending much time in the coming years and decades. Within NASA the Spacecraft Radiation Health Program at Johnson Space Center (http://sn-io.jsc.nasa.gov/sreg/techmemo.htm) leads in the research and development activities that address the health effects of space radiation exposure to astronauts. Astronauts carry personal radiation dosage badges and radiation monitors are located throughout the shuttle. There is a space radiation analysis group (SRAG) which predicts, in real time, the exposure that might occur during a solar flare and terminates extravehicular activity if that is necessary.

It is impossible to predict how much radiation an astronaut will receive, although one can make an estimate of the probability of receiving a given amount. However, there is a chance that these limits will be exceeded in space. NASA regulations for limits of exposure, measured in REM's, call for 15 REM for 30 day exposure, 50 REM for annual exposure, 150 to 400 REM for exposure for men (more REM with increasing age), 100 to 300 for exposure for women (more REM with increasing age).

The radiation environment experienced by astronauts on Skylab and cosmonauts on Mir, as a function of their geographic location, has been studied by Badhwar (1997). Figure 16 shows figures from that paper, clearly illustrating that there is a major peak in radiation at the SAA, although there are minor peaks in other places. The 300 nGy/min peak over the SAA corresponds to about 30 mRad/min (30 mREM/min). Figure 8 shows the line of force cut by the shuttle, which is at 480 km altitude, orbital inclination 28.5 degrees. Although this line is steeply inclined to the vertical, the shuttle is well beyond the sensible atmosphere. The average value of radiation in the SAA is less than this peak value and is about half of this or 15 mREM/min. An astronaut would have to spend 1000 minutes (17 hrs) in the SAA during 30 days to reach his/her exposure limit. For a U.S. astronaut or Russian cosmonaut who stays in space for a year, perhaps on the space station, there is the 50 REM annual limit (note that is much less than 12 times the monthly limit). The radiation dosage of astronauts on the space station will be continuously monitored from Earth. During their flights to and from the moon the Apollo astronauts were lucky because they would have received a lethal dose of radiation if a strong solar event had occurred while they were in space—and such disturbances occur several times per year. A recent National Academy of Science study (National Academy of Science, 1996) showed that manned flights to Mars, because they are of long duration and outside the shielding of the magnetosphere, will not be possible, regardless of wishful thinking, until the shielding problem can be solved.

It is interesting to note that TOPEX, at an altitude of 1334 km, inclination 63 degrees, spent 42 minutes in the SAA over a 3-year period (14 min/yr). It received 2.3 rad per orbit or an accumulated dose of 12,000 rad/yr behind 1 gm/cm^2 Al shielding. This is far in excess of the lifetime limits for humans.

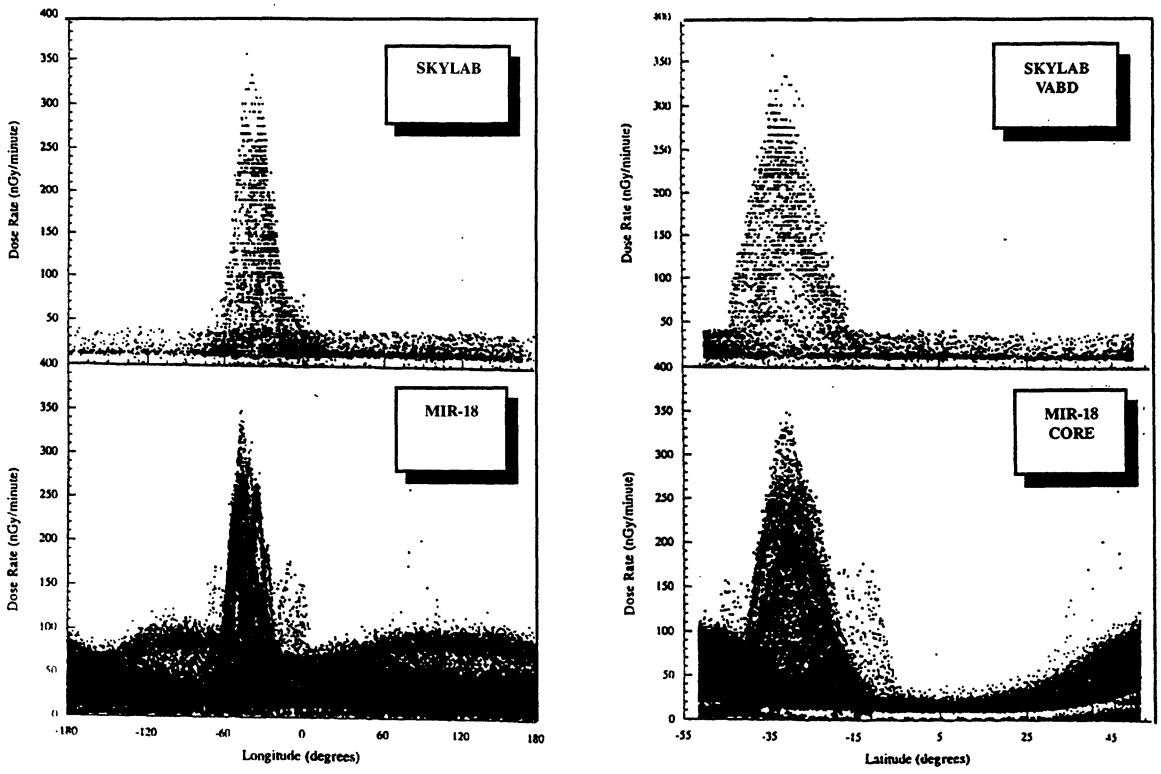

Figure 16. Distribution of dose rates as functions of latitude and of longitude for Skylab (Dec. 1973–Jan. 1974) and for Mir (Mar. 1995). Mir's results were adjusted to Skylab's to compensate for altitude difference (after Badhwar (1997)).

Shuttle flights with a 28.5 degree inclination do not pass through the entire SAA. Shuttle flights with 57 degree inclination do pass through the entire SAA but receive less radiation because they spend less time in the SAA.

THE FUTURE OF THE SOUTH ATLANTIC ANOMALY

Since the geomagnetic field is not static it is worthwhile investigating what the SAA and associated radiation hazard might be in the future. Figure 17 shows the secular change in total intensity of the field for the year 1995, as given by the IGRF. It shows that the greatest rate of decrease of the field is in the South Atlantic southwest of Capetown where the secular variation is more than 100 nT/yr. There is a secondary area of rapidly decreasing field in the western North Atlantic where it exceeds 80 nT/yr. Measurements over the past century, for much of the world, show essentially the same rate of change as for 1995 (Sabaka, et al., 1997). It is understood that data taken at some specific locations will differ from those shown by the spherical harmonic contours since the process of generating the spherical harmonic coefficients will possibly smooth over all values to fit a spherical harmonic expression.

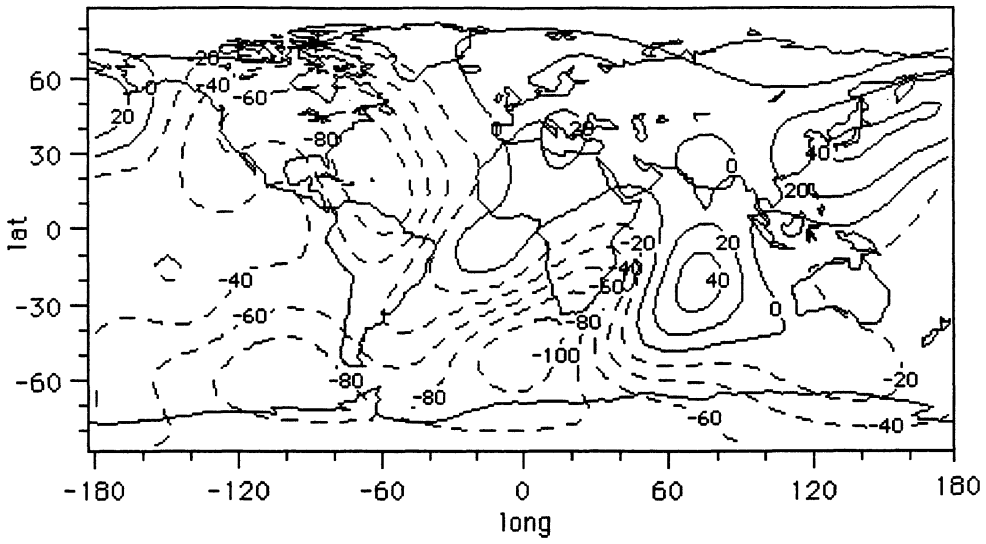

Figure 17. Secular variation of total field (in nT/yr) from IGRF model.

Precisely extrapolating the rate of change of the geomagnetic field into the future is impossible because the reason for change is unknown. Here we can only draw upon what has happened in the past and assume that will continue for the next few decades. For some observatories, especially in the Northern Hemisphere, and in India, the slope of field strength vs time has shown a complete change of slope in the past. Many investigators have not tried to predict the field in the face of this erratic behavior. For the SAA region we can look at the records from 11 observatories that exist around the South Atlantic region. Those with records extending for more than 25 years are listed in table 2, and their locations shown in figure 18. Table 2 also gives the period of time for which there are yearly mean records and the rate of change of total field that those records show, calculated from a least-squares fit to a straight line. These data were obtained from NGDC. Figure 18 also shows the data for five observatories with the longer records and illustrates that the field is changing at a constant rate. Comparing these rates of change to figure 17 it is seen that the change at Hermanus (HER) and Syowa Base (SYO) are greater than figure 17 shows, but other observatories are about the same as the global map of figure 17 indicates.

Table 2. Secular variation of the total field at observatories around the South Atlantic.

Annual Means From NGDC Annual Means Web Database:			
Code	**Sec, Var. (nT/yr)**	**Years**	**Name**
HER	-110.4	1940–1999	Hermanus, S. Africa
KOU	-105.4	1958–1975	Surinam
LAS	-46.7	1965–1995	Las Acacias, Argentina
LQA	-47.4	1928–1987	La Quiaica, Argentina
MBO	-14.5	1952–1988	M'Bour, Senegal
PIL	-57.6	1905–1997	Pilar, Argentina
SYO	-101.3	1955–1997	Syowa Base, Antarctica
TRW	-77.9	1958–1995	Trelew, Argentina
TSU	-57.7	1952–1997	Tsumba, Namibia
TTB	-69.2	1960–1992	Tatuoca, Brazil
VSS	-25.2	1920–1997	Vassouras, Brazil
Annual Means From IGPP Monthly Means Web Database:			
HER	-87.4	1992–1994.8	Hermanus, S. Africa
HER	-81.4	1995–1998.5	Hermanus, S. Africa
LAS	-65.1	1992–1994.6	Las Quiaica, Argentina
TSU	-59.6	1992.2–1994.9	Tsumba, Namibia
TSU	-65.6	1995–1998.5	Tsumba, Namibia

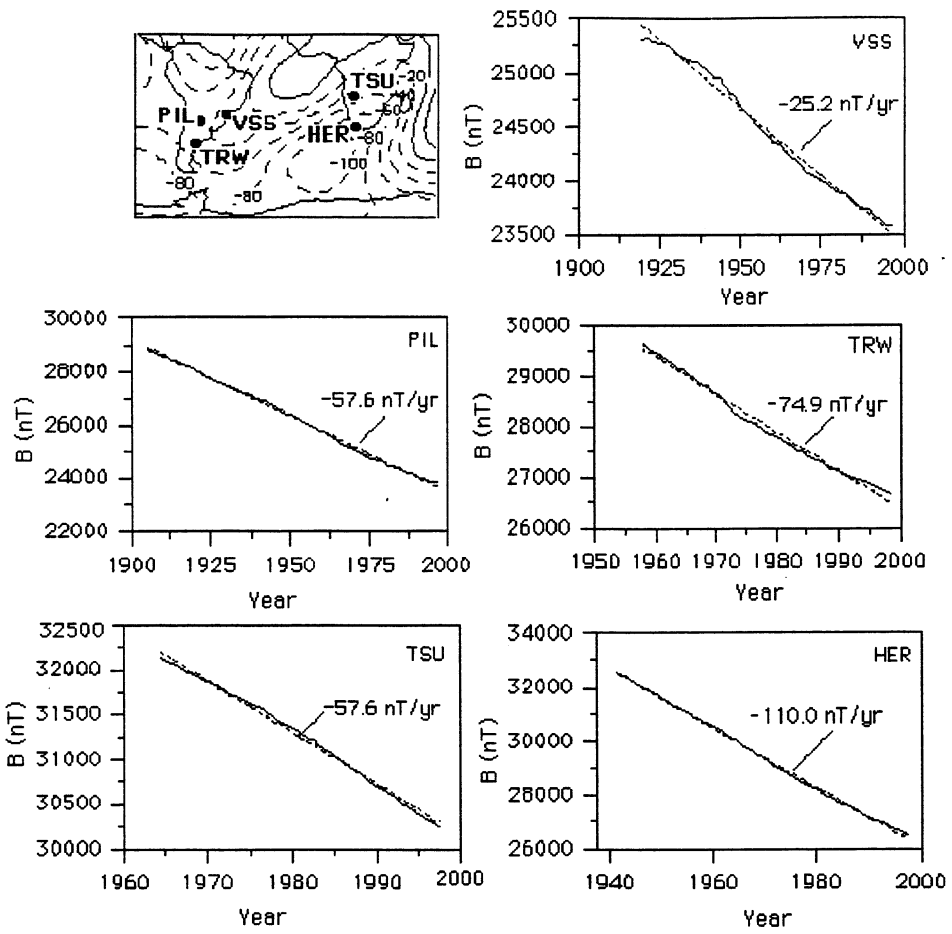

Figure 18. Secular variation of total field as observed at longer operating geomagnetic observatories around the South Atlantic. The location of the observatories is shown in the upper left, with secular change from figure 17 superimposed. A least-squares fit of the observed data to a straight line is shown with the slope of that line indicated.

Also in table 2 we give rates of change calculated from *monthly* mean values, for some observatories, with the data obtained from IPGP Paris (http://obsmag.ipgp.jussieu.fr/AM-rqobsmag.html). The monthly mean data only extends for the last 8 years and does not follow so smooth a curve as the yearly means. The slope of these curves was also determined by a least-square fit to a straight line and those slopes are given in table 2. It is seen that the monthly means for Hermanus give values closer to the values in figure 17, than does the yearly mean. This suggests that, in the last few years, the field at Hermanus and Syowa Base may have been decreasing faster than at earlier times.

For periods of time longer than shown in table 2 one might think of the geologic record of the paleomagnetic field. Kreer et al. (1983) reported on a paleomagnetic study of Argentine lake sediments from each of three adjacent lakes located about 600 km northwest of the Trelew geomagnetic observatory. The sediments from one of the lakes extended back 14,000 years, but sediments from the other lakes did not extend back so far. The declination and inclination records from the three lakes could be stacked to produce a record of the direction of the field for the last 6,000 years. The probable error of these directions is high although they show a large excursion to the west and up about 500 years ago.

The authors show intensity and susceptibility profiles from eight cores from the three lakes but were unable to make a stacked intensity profile because of the high variability from lake to lake. From the figures shown the intensity seems to have varied erratically by 10 to 20 percent with numerous short excursions of intensity, which can easily be artifacts. The authors point out that these are the first paleomagnetic measurements from South America and much remains to be done before measurements like this have high reliability. A search of the literature did not reveal any paleomagnetic measurements from lakes from South Africa.

The Deep Sea Drilling Project and the International Program of Ocean Drilling have drilled a number of holes in the South Atlantic Ocean floor. Magnetic measurements are usually made on the deep-sea core material but, contrary to cores from the North Atlantic, no comprehensive report of paleomagnetic intensities has been made for the South Atlantic. In any case, the sedimentation rate in the oceans is usually much slower than in lakes, and time scale so compressed, they are not likely to yield information relevant to the last few hundred years.

It is clear that the spherical harmonic model of the field and its secular change smoothes the field and cannot be expected to give exactly correct values at all points on the Earth. For purposes of this report we will assume that the rate of change as illustrated in figure 17 is correct enough to be used to extrapolate tens to a few hundred years in the future. The calculation is carried out by updating each of the spherical harmonic coefficients, according to their first-time derivative, calculating the X, Y, and Z components of the field and then calculating B from X, Y, and Z.

Figure 19 shows the total field for the year 1995 extrapolated to the years 2025, 2050, and 2100. The principle feature of the geomagnetic field is the change in the SAA. Each few decades it gets larger and the field within it gets weaker. A secondary low shows southwest of Capetown.

One may define the extent of the SAA by the areal extent of the high dose rates for shuttle and Mir (figure 16). The high dose rates extend from approximately 15 S to 40 S and from 20 W to 70 W at 480 km altitude. This corresponds roughly to the 25,000 nT contour on the Earth's surface. Using this contour to identify the SAA, in the year 2100 the SAA will cover most of South America, the southern part of Africa and the South Atlantic Ocean south of 25 S to the Scotia Sea and Antarctica. The size of the SAA will have increased by a factor of about 4. This suggests that the radiation hazard to humans in space may be increased by a corresponding amount. This will mean that astronauts can spend correspondingly less time in space.

In 1995, the focus of the SAA was clearly over the coast of Brazil. In 2100 there will be two foci: one in northern Brazil and a second and deeper one southwest of Capetown in the South Atlantic Ocean.

Radiation levels with this new SAA will be different from the present for two reasons: (1) because the field is less and the mirror points of particles lower with more being lost to the atmosphere (greater bounce cone loss), and (2) as mentioned before, the area of this low field will be greater than it is now. The first effect would probably reduce the level of radiation, while the second effect would tend to distribute the radiation over a larger area with the integrated effect increasing the radiation hazard. It is tacitly assumed that at present the radiation belts are in approximate equilibrium with the input of particles from

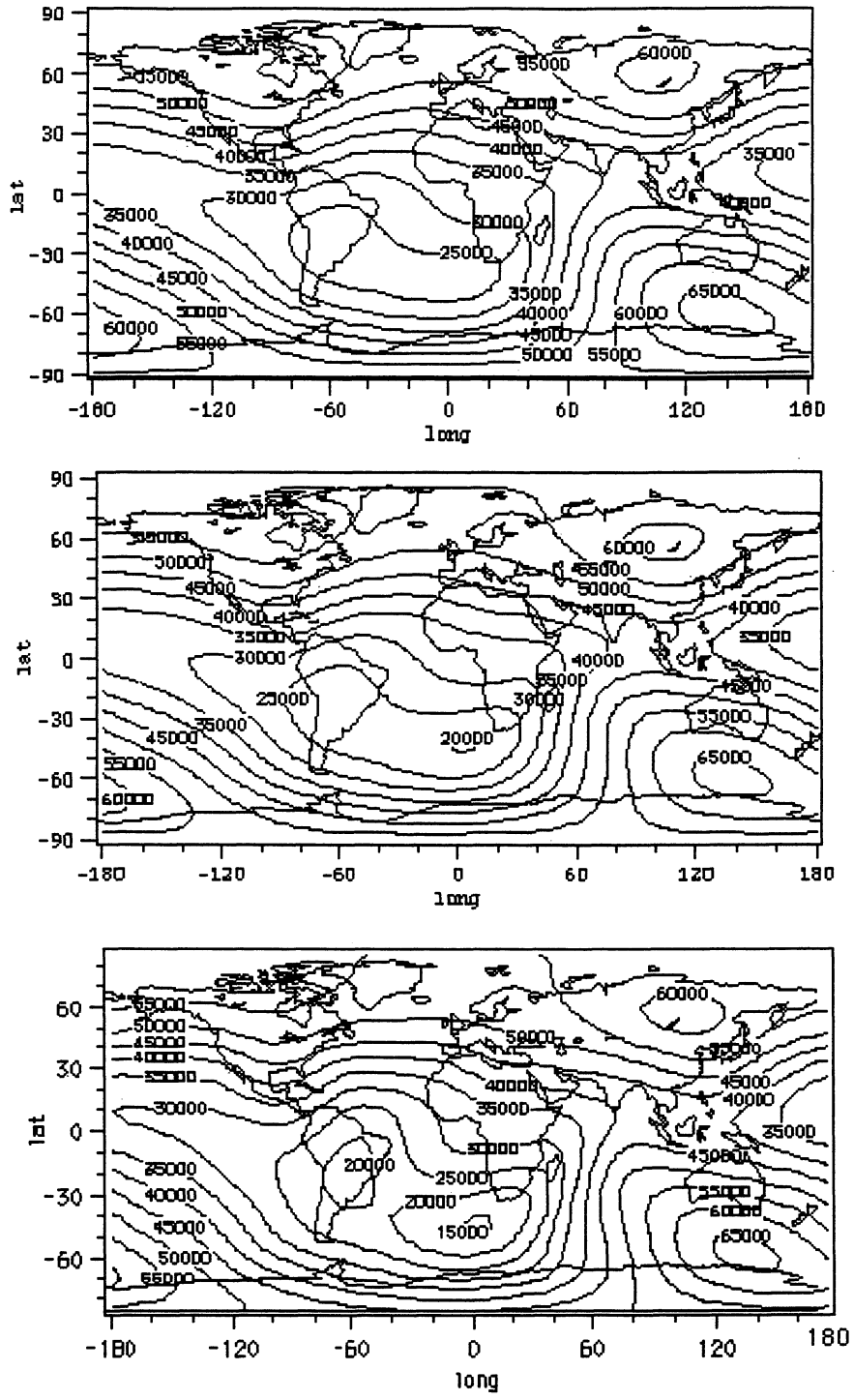

Figure 19. Total field contour map (in nT) for the years 2025 (upper), 2050 (center), and 2100 (lower) extrapolated from IGRF 95.

galactic and solar sources balancing the number of particles lost by atmospheric scattering. In the future the sources would be the same as today while the losses would be greater. This could seriously deplete the particle population of the radiation belts. Able and Thorne, 1999, have made progress in quantifying the factors which create a radiation hazard over the SAA in 1995. A similar analysis for a possible future field is needed with attention given to the balance between the source supply and the atmospheric loss.

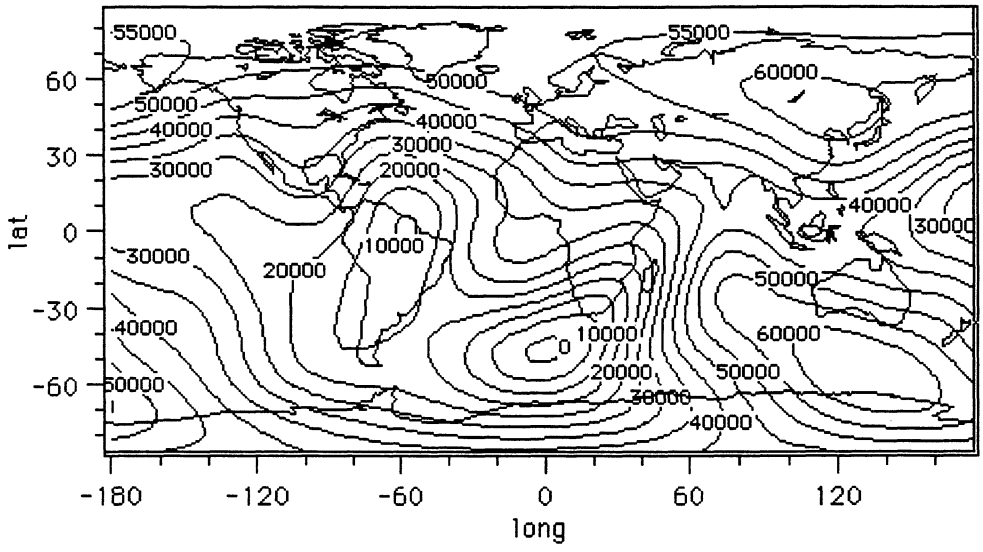

Figure 20. Total field contour map (in nT) for the year 2235, extrapolated from IGRF 95.

It is interesting to continue to extrapolate the field 240 years in the future, to the year 2235. The focus in northern South America intensifies but the field strength approaches zero in the South Atlantic (figure 20). Naturally, all components of the field (X, Y, H, and Z) must approach zero if the total field approaches zero. This does not constitute a global reversal of the geomagnetic field but is a phenomenon confined to the South Atlantic, at that time.

Using the 1995 IGRF secular change in inclination one may calculate how the geomagnetic equator (where the field is horizontal) will change with time. Figure 21 shows that the geomagnetic equator in the Atlantic will move north by 10 to 15 degrees in the next 100 years and by 15 to 30 degrees in the next 240 years. In other parts of the world the change is not great, although it may change long-range high-frequency radio transmissions.

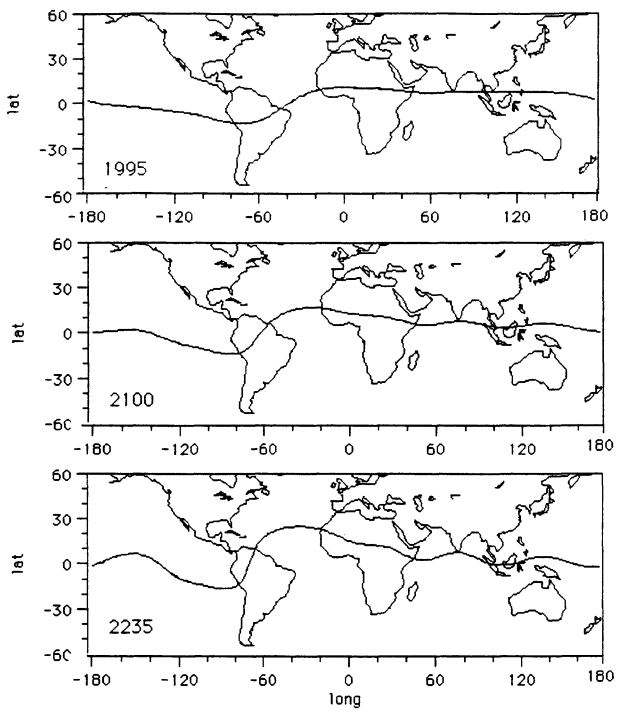

Figure 21. Location of geomagnetic equator (where dip is zero) for years 1995, 2100, and 2235 all based on IGRF 95.

REFERENCES

Abel, Bob, and Richard M. Thorne, Modeling energetic electron precipitation near the South Atlantic anomaly, *Jour. Geophy. Res.*, **104**, 7037–7044, 1999.

Badhwar, G.D., V.A. Shurshakov, and V. V. Tsetlin, Solar Modulation of Dose Rate Onboard the Mir Station, *Trans. Nuc. Sci.*, **44**, 2529–2541, 1997.

Barton, C.E., and members of Working Group 8, International geomagnetic reference field, 1995 revision, International Association of Geomagnetism and Aeronomy (IAGA) Division V, Working Group 8, *Geophys. J. Int.*, **125**, 318–321, 1996.

Cain, J.C, R.A. Langel, and S.J. Hendricks, Magnetic Chart of the Brazilian Anomaly—A Verification, *Geomag. and Aeronomy,* **8**, 1, 84–87, 1968.

Dessler, A.J., and Robert Kaplan, Some properties of the Van Allen radiation, *Phy. Rev. Ltrs.*, **6**, 271–274, 1960.

Fung, S.F., Recent developments in the NASA trapped radiation models, pp. 79–91, in Radiation Belts: Models and Standards, J.F. Lemaire, D. Heynderickx, and D.N. Baker, Eds. *AGU Geophysical Monograph,* **97**, 1996.

Heirtzler, James R. and J. Hirshman, Measurements of the geomagnetic field near Capetown, *Jour. of Geophys. Res.*, **65**, 3016–3018, 1960.

Kreer, K.M., D.A. Valencio, A.M. Sinito, P. Tucholka and J.F.A. Vilas, Geomagnetic secular variations 0–14000 yr BP as recorded by lake sediments from Argentina, *Geophys. J. R. Astr. Soc.*, **74**, 199–221, 1983.

McIlwain, Carl E., Coordinates for mapping the distribution of magnetically trapped particles, *Jour. of Geophys. Res.*, **66**, 3681–3691, 1961.

Mlodnosky, R.F., and R.A. Helliwell, Graphic data on the Earth's main magnetic field in space, *Jour. of Geophys. Res.*, **67**, 1962.

National Academy of Science, Radiation hazards to crews of interplanetary missions, Biological Issues and Research Strategies, by Task Group on the Biological Effects of Space Radiation, National Academy Press, Washington, D.C., 75 pp., 1996.

Quinn, John M., Rachel J. Coleman, Donald L. Shiel, John M. Nigro, Joint US/UK 1995 Epoch World Magnetic Model, Naval Oceanographic Office, Technical Report TR 314, Stennis Space Center, April 1995.

Sabaka, T.J., R.A. Langel, R.T. Baldwin, and J.A. Conrad, The geomagnetic field 1900–1995, including the large-scale field from magnetospheric sources and the NASA candidate models for the 1995 revision of the IGRF, *J. Geomag. Geoelectr.* **49**, 157–206, 1997.

Roederer, J.G., Dynamics of geomagnetically trapped radiation, Springer-Verlag, New York, 166 pp., 1970.

U.S. Standard Atmosphere, NOAA-S/T 76-1562, U.S. Government Printing Office, 1976.

Walt, Martin, Introduction to geomagnetically trapped radiation, Cambridge University Press, 168 pp., 1994.

Wilson, J.W., J. Miller, A. Konradi, and F.A. Cucinotte, Shielding strategies for human space exploration, NASA Conference Publication 3360, December 1997.

APPENDIX

This computer code, in True Basic, will plot the field strength B or altitude h vs latitude, with mirror points indicated (similar to figure 11) or it can be modified to make a number of the other plots shown in this report. Note that most of this code, after statement 2400, is the subroutine GEOMAGJ to calculate the field components for a given latitude, longitude, and altitude. The file "IGRF95" is called for in the sub-routine and a sample listing of values in this file is given following the listing of the main program. Also note that a large number of lines is to calculate the location of the mirror points and plot them. This part can be skipped by inserting a "Go to" statement and this will materially reduce the number of lines.

```
10 !Computer code  plot B or h vs lat with mrror pts.
20 !Written in TrueBasic, Nov 1998, JRH
30 !stores graphics on clipboard
40 set zonewidth 6
50 OPTION NOLET
60 OPTION ANGLE degrees
70 DIM h(200),lt(200),ln(200),b(200),dp(200),dc(200)   !for pts along line of force
80 DIM bm(100)                    !for field values at mirror points
90 DIM hms(100),ltms(100),lnms(100),bms(100)   !for variables at mirror pts in south hemisphere
100 DIM hmn(100),ltmn(100),lnmn(100),bmn(100)   !for variables at mirror pts in north hemisphere
110 !OPEN#4: NAME OUTFILE$,CREATE NEW,ORG TEXT
120 !             ***** initialize for plotting *****
130 LIBRARY "PictLib*"
140 LIBRARY "MacTools*"
150 call Copy_clipboard
160 open#2: screen .05,.4,.05,.6   !to make "trim" fit
170 xmin=-55
180 xmax=55
190 ymin=0
200 ymax=10000
210 set window xmin,xmax,ymin,ymax
220 !             ***** draw box *****
230 plot lines: xmin,ymin;xmax,ymin
240 plot lines: xmax,ymin;xmax,ymax
250 plot lines: xmax,ymax;xmin,ymax
260 plot lines: xmin,ymax;xmin,ymin
270 !             ***** plot tics on y axis *****
280 for n=ymin to ymax step 1000
290 plot lines: xmin,n;xmin+1,n
300 plot lines: xmax-1,n;xmax,n
310 next n
320 !             ***** plot tics on x axis *****
330 for n=xmin to xmax step 5
340 plot lines: n,ymin;n,ymin+100
350 plot lines: n,ymax-100;n,ymax
360 next n
370 !             ***** calculate and plot field line *****
380 !
```

```
390 dlat=1      !lat increment along path, deg
400 for flonk=0 to 0 !step 30   !this steps longitude of origin
410 for nk=-50 to -30 step 10   !this steps latitude of origin
420 flatmin=nk   !starting lat, deg
430 flatmax=-nk   !final lat, deg
440 alt1=0      !starting alt, km
450 flat1=flatmin
460 flon1=flonk
470 k=1
480 flat=flat1
490 alt=alt1
500 flon=flon1
510 !
520 !           ***** stepping along path begins here *****
530 !
540 CALL GEOMAGJ (alt,flat,flon,t,dip,dec)  !get value of t,dip, dec
550 h(k)=alt
560 lt(k)=flat
570 ln(k)=flon
580 b(k)=t
590 dp(k)=dip
600 dc(k)=dec
610 k=k+1
620 dalt=-110*dlat*tan(dip)
630 alt=alt+dalt
640 alt2=alt
650 if alt2<0 then go to 1050  ! if alt goes into ground we have gone too far
660 flat2=flat1+dlat
670 dlon=110*dlat*tan(dec/60)
680 flon2=flon1+dlon
690 go to 1000
700 if flon1>180 then   ! change from flon,flat to x,y
710 x1=flon1-360
720 go to 810
730 else
740 if flon1<-180 then
750 x1=flon1+360
760 go to 810
770 else
780 x1=flon1
790 end if
800 end if
810 y1=flat1
820 if flon2>180 then
830 x2=flon2-360
840 go to 930
850 else
860 if flon2<-180 then
870 x2=flon2+360
880 go to 930
890 else
900 x2=flon2
910 end if
920 end if
930 y2=flat2
```

```
940 if x2>xmax or x2<xmin then go to 1000   !out of bounds
950 if y2>ymax or y2<ymin then go to 1000   !out of bounds
960 base=abs(x1)+abs(x2)
970 if base>=358 then go to 1000   !to prevent line from jumping from one side to the other
980 !if alt2<600 then box circle x1-.5,x1+.5,y1-.5,y1+.5  !emphase line is alt is low
990 plot lines: x1,y1;x2,y2  !plot line segment
1000 flat1=flat2   !advance points
1010 flon1=flon2
1020 alt1=alt2
1030 go to 480
1040 !         ***** plot b(n) or h(n) vs lt(n) from n=1 to kmax *****
1050 kmax=k-1
1060 xx1=-lt(1)
1070 yy1=h(1)
1080 for n=2 to kmax
1090 xx2=-lt(n)
1100 yy2=h(n)
1110 plot lines: xx1,yy1;xx2,yy2
1120 xx1=xx2
1130 yy1=yy2
1140 next n
1150 !         ***** find values for dip equator *****
1160 !
1170 for k=1 to kmax-1    !this loop ends on line 1470
1180 if dp(k)<=0 and dp(k+1)>0 then
1190   factor=abs(dp(k)/(dp(k+1)-dp(k)))
1200   if h(k+1)<=h(k) then
1210     heq=h(k)-factor*(abs(h(k+1)-h(k)))  !alt decreasing or no change
1220   else
1230     heq=h(k)+factor*abs((h(k+1)-h(k)))  !alt increasing
1240   end if
1250   lteq=lt(k)+factor*(lt(k+1)-lt(k))  !lat is always increasing
1260   if ln(k+1)<=ln(k) then
1270     lneq=ln(k)-factor*abs((ln(k+1)-ln(k)))  !long is decreasing or no change
1280   else
1290     lneq=ln(k)+factor*abs((ln(k+1)-ln(k)))  !long is increasing
1300   end if
1310   if b(k+1)<=b(k) then
1320     beq=b(k)-factor*abs((b(k+1)-b(k)))  !b is decreasing or no change
1330   else
1340     beq=b(k)+factor*abs((b(k+1)-b(k)))  !b is increasing
1350   end if
1360   if dp(k+1)<=dp(k) then
1370     dpeq=dp(k)-factor*abs((dp(k+1)-dp(k)))  !dip is decreasing or no change
1380   else
1390     dpeq=dp(k)+factor*abs((dp(k+1)-dp(k)))  !dip is increasing
1400   end if
1410   if dc(k+1)<=dc(k) then
1420     dceq=dc(k)-factor*abs((dc(k+1)-dc(k)))  !declination is decreasing or no change
1430   else
1440     dceq=dc(k)+factor*abs((dc(k+1)-dc(k)))  !declination is increasing
1450   end if
1460 end if
1470 next k
1480 !
```

```
1490 !        ***** calc south and north mirror pts for eq pitch angle alpha *****
1500 !
1510 for alpha=80 to 30 step -10  !this loop ends at statement 2140
1520 bm(alpha)=beq/(sin(alpha)*sin(alpha))  !value of bm for this alpha
1530 !
1540 !        *****  search for and plot  mirror pts, first south of eq, then north  *****
1550 !
1560    for k=1 to kmax-1  !start following along line of force,ends at statement 2130
if dp(k)<=0 then   !south of mag equator
1580        if b(k)>=bm(alpha) and b(k+1)<bm(alpha) then   !value found, calcuate
1590         factor=abs((bm(alpha)-b(k))/(b(k+1)-b(k)))
1600         if h(k+1)<=h(k) then
1610          hms(alpha)=h(k)-factor*(abs(h(k+1)-h(k)))  !h is decreasing
1620         else
1630          hms(alpha)=h(k)+factor*abs((h(k+1)-h(k)))    !h is increasing
1640         end if
1650         ltms(alpha)=lt(k)+factor*(lt(k+1)-lt(k))
1660         if ln(k+1)<=ln(k) then
1670          lnms(alpha)=ln(k)-factor*abs((ln(k+1)-ln(k)))    !ln is decreasilng
1680         else
1690          lnms(alpha)=ln(k)+factor*abs((ln(k+1)-ln(k)))    !ln is  increasing
1700         end if
1710         if b(k+1)<=b(k) then
1720          bms(alpha)=b(k)-factor*abs((b(k+1)-b(k)))    !b is decreasing
1730         else
1740          bms(alpha)=b(k)+factor*abs((b(k+1)-b(k)))    !b is increasing
1750         end if
1760         x1=ltms(alpha)-1  !plot lat, h box around south mirror pt
1770         x2=ltms(alpha)+1
1780         y1=hms(alpha)-50
1790         y2=hms(alpha)+50
1800        if hms(alpha)<>0 then box circle -x2,-x1,y1,y2   !draw box 1
1810        else    !value not found
1820         go to 2130  !continue search south of mag equator
1830        end if    !end calc for south mirror pt
1840      else        !north of mag equator
1850        if b(k)<bm(alpha) and b(k+1)>=bm(alpha) then !value found, calculate
1860         factor=abs((bm(alpha)-b(k))/(b(k+1)-b(k)))
1870         if h(k+1)<=h(k) then
1880          hmn(alpha)=h(k)-factor*(abs(h(k+1)-h(k)))    !h is decreasing
1890         else
1900          hmn(alpha)=h(k)+factor*abs((h(k+1)-h(k)))    !h is increasing
1910         end if
1920         ltmn(alpha)=lt(k)+factor*(lt(k+1)-lt(k))
1930         if ln(k+1)<=ln(k) then
1940          lnmn(alpha)=ln(k)-factor*abs((ln(k+1)-ln(k)))   !ln is decreasing
1950         else
1960          lnmn(alpha)=ln(k)+factor*abs((ln(k+1)-ln(k)))    !ln is increasing
1970         end if
1980         if b(k+1)<=b(k) then
1990          bmn(alpha)=b(k)-factor*abs((b(k+1)-b(k)))    !b is decreasing
2000         else
2010          bmn(alpha)=b(k)+factor*abs((b(k+1)-b(k)))    !b is increasing
2020         end if
2030         x1=ltmn(alpha)-1  !plot lat, h box around north mirror pt
```

```
2040          x2=ltmn(alpha)+1
2050          y1=hmn(alpha)-50
2060          y2=hmn(alpha)+50
2070          if hmn(alpha)<>0 then box circle -x2,-x1,y1,y2  !draw box 2
2080         else     !value not found, continue north of mag equator
2090          go to 2130
2100       end if      !ends calc north mirror pt
2110       go to 2140   !jump out of this loop and finish this search
2120      end if       !ends test of dip
2130      next k       !ends checking line of force for this value of alpha
2140 next alpha
2150 for alpha= 80 to 40 step -10   !plot marks for mirror pts
2160 if hms(alpha)<>0 then
2170  xx1=-ltms(alpha)-.5  !plot lat, b box around south mirror pt
2180  xx2=-ltms(alpha)+.5
2190  yy1=bms(alpha)-300
2200  yy2=bms(alpha)+300
2210  !box circle xx1,xx2,yy1,yy2    !draw  box 3
2220 else
2230  go to 2250
2240 end if
2250 if hmn(alpha)<>0 then
2260  xx3=-ltmn(alpha)-.5  !plot lat, b box around north mirror pt
2270  xx4=-ltmn(alpha)+.5
2280  yy3=bmn(alpha)-300
2290  yy4=bmn(alpha)+300
2300  !box circle xx3,xx4,yy3,yy4   !draw box 4
2310 else
2320  go to 2340
2330 end if
2340 next alpha
2350 next nk
2360 next flonk
2380 call Copy_done
2390 close #2
2400 END
2410 !        ***** END OF PROGRAM *****
2420 !
2430 !        ***** subroutine to calculate field components *****
2440 SUB GEOMAGJ(alt,flat,flon,t,dip,dec)
2450   !subroutine GEOMAGJ to calc geomag field components from coefs
2460   !read in coefs and sec change, after sub getshc of NGDC
2470   option nolet
2480   option angle degrees
2490   dim gh(224)
2500   dim dgh(224)
2510   ddate=2100.0
2520   infile$="IGRF95"
2530   factor=ddate-1995.0
2540   nmax=10
2550   open #3:name infile$
2560    i = 0
2570    for nn = 1 to nmax
2580      for mm = 0 to nn
2590      input#3:m,n,g,h,dg,dh
```

```
2600          i = i + 1
2610          gh(i) = g
2620          dgh(i)= dg
2630          if (m <> 0) then
2640            i = i + 1
2650            gh(i) = h
2660            dgh(i)=dh
2670          end if
2680    next mm
2690    next nn
2700    close #3
2710    !
2720    !
2730    !input:
2740    !   igdgc - indicates coordinate system used; set equal to
2750    !         1 if geodetic, 2 if geocentric
2760    !   flat  - north latitude, in degrees
2770    !   flon  - east longitude, in degrees
2780    !   elevkm  - elevation above mean sea level (igdgc=1), or
2790    !           radial distance from earth's center (igdgc=2)
2800    !   erad  - value of earth's radius associated with the sh
2810    !           coefficients, in same units as elevkm
2820    !   a2,b2 - squares of semi-major and semi-minor axes of
2830    !           the reference spheroid used for transforming
2840    !           between geodetic and geocentric coordinates or
2850    !           components
2860    !  nmax  - maximum degree and order of coefficients
2870    !  gh    - schmidt quasi-normal internal spherical
2880    !           harmonic coefficients
2890    !
2900    ! output:
2910    !  x    - northward component
2920    !  y    - eastward component
2930    !  z    - vertically-downward component
2940    !
2950    !based on subroutine 'igrf' by d. r. barraclough and
2960    !s. r. c. malin, report no. 71/1, institute of geological
2970    !sciences, u.k.
2980    !
2990    dim  sl(14), cl(14)   ! here set for nmax=14
3000    dim p(119), q(119)
3010    dim ext(3)
3020    ! ========================================================
3030    !igdgc=2  !geocentric coord., elevkm=dist from earth center
3040    igdgc=1   ! geodetic coord., elevkm=elev above mean sea level
3050    elevkm=alt
3060    erad=6371.2
3070    a2=40680925.
3080    b2=40408588.
3090    dtr = .01745329
3100    r = elevkm
3110    slat = sin (flat)
3120    if (90. - flat) < .001 then
3130       aa = 89.999
3140    !   300 ft from n. pole
```

```
3150   else if (90. + flat) < .001 then
3160      aa = -89.999
3170   !   300 ft from s. pole
3180   else
3190      aa = flat
3200   end if
3210   clat = cos (aa)
3220   sl(1) = sin (flon)
3230   cl(1) = cos (flon)
3240   x = 0.
3250   dx=0.
3260   y = 0.
3270   dy=0.
3280   z = 0.
3290   dz=0.
3300   sd = 0.
3310   cd = 1.
3320   n = 0
3330   l = 1
3340   m = 1
3350   npq = (nmax * (nmax + 3)) / 2
3360   if igdgc = 1 then
3370      aa = a2 * clat * clat
3380      bb = b2 * slat * slat
3390      cc = aa + bb
3400      dd = sqr (cc)
3410      r = sqr (elevkm * (elevkm + 2. * dd)+(a2 * aa + b2 * bb) / cc)
3420      cd = (elevkm + dd) / r
3430      sd = (a2 - b2) / dd * slat * clat / r
3440      aa = slat
3450      slat = slat * cd - clat * sd
3460      clat = clat * cd + aa * sd
3470   end if
3480   ratio = erad / r
3490   aa = sqr (3.)
3500   p(1) = 2. * slat
3510   p(2) = 2. * clat
3520   p(3) = 4.5 * slat * slat - 1.5
3530   p(4) = 3. * aa * clat * slat
3540   q(1) = -clat
3550   q(2) = slat
3560   q(3) = -3. * clat * slat
3570   q(4) = aa * (slat * slat - clat * clat)
3580   for k = 1 to npq  ! this loop ends at statement 4110
3590      if n < m then
3600         m = 0
3610         n = n + 1
3620         rr = ratio^(n + 2)
3630         fn = n
3640      end if
3650      fm = m
3660      if k >= 5 then
3670         if m = n then
3680            aa = sqr (1. - .5 / fm)
3690            j = k - n - 1
```

```
3700            p(k) = (1. + 1. / fm) * aa * clat * p(j)
3710            q(k) = aa * (clat * q(j) + slat / fm * p(j))
3720            sl(m) = sl(m-1) * cl(1) + cl(m-1) * sl(1)
3730            cl(m) = cl(m-1) * cl(1) - sl(m-1) * sl(1)
3740          else
3750            aa = sqr (fn * fn - fm * fm)
3760            bb = sqr ((fn - 1.)^2 - fm * fm) / aa
3770            cc = (2. * fn - 1.) / aa
3780            i = k - n
3790            j = k - 2 * n + 1
3800       p(k) = (fn + 1.) * (cc * slat / fn * p(i) - bb/ (fn - 1.) * p(j))
3810       q(k) = cc * (slat * q(i) - clat / fn * p(i))- bb * q(j)
3820         end if
3830       end if
3840       aa = rr * gh(l)
3850       daa= rr * dgh(l)
3860       if m = 0 then
3870          x = x + aa * q(k)
3880          dx= dx + daa * q(k)
3890          z = z - aa * p(k)
3900          dz = dz - daa*p(k)
3910          l = l + 1
3920       else
3930          bb = rr * gh(l+1)
3940          dbb = rr * dgh(l+1)
3950          cc = aa * cl(m) + bb * sl(m)
3960          dcc = daa * cl(m) + dbb * sl(m)
3970          x = x + cc * q(k)
3980          dx = dx + dcc * q(k)
3990          z = z - cc * p(k)
4000          dz = dz - dcc * p(k)
4010          if clat > 0. then
4020          y = y + (aa * sl(m) - bb * cl(m)) * fm * p(k)/ ((fn + 1.) * clat)
4030          dy = dy + (daa * sl(m) - dbb * cl(m)) * fm * p(k)/ ((fn + 1.) * clat)
4040          else
4050             y = y + (aa * sl(m) - bb * cl(m)) * q(k)* slat
4060             dy = dy + (daa * sl(m) - dbb * cl(m)) * q(k)* slat
4070          end if
4080          l = l + 2
4090       end if
4100       m = m + 1
4110       next k
4120       x = x + factor * dx
4130       y = y + factor * dy
4140       z = z + factor * dz
4150    aa = x
4160    x = x * cd + z * sd
4170    z = z * cd - aa * sd
4180    h=sqr(x*x+y*y)
4190    sn=0.0001
4200    rad=57.29577951
4210    t=sqr(x*x+y*y+z*z)
4220    if x=0 and y=0 then dec=0
4230    if x=0 and y<0 then dec=-90
4240    if x=0 and y>0 then dec=90
```

```
4250  ayx=(y/x)
4260   if x>0 and y<0 then dec=(atn(ayx))
4270   if x<0 and y<0 then dec=(atn(ayx)-180)
4280   if x<0 and y>0 then dec=(180-atn(ayx))
4290   if x>0 and y>0 then dec=(atn(ayx))
4300   if h=0 and z=0 then dip=0
4310   if h=0 and z>0 then dip=-90
4320   if h=0 and z<0 then dip=90
4330   azh=(z/h)
4340   if z=0 then dip=0
4350   if z>0 then dip= abs(atn(azh))
4360   if z<0 then dip= -abs(atn(azh))
4370   end sub
```

The following is a listing of the contents of file "IGRF95" called for in the subroutine GEOMAGJ. Only coefficients through nmax=5 are illustrated here. The sequence is as shown below.

m	n	g	h	dg	dh
0	1	-29682	0	17.6	0
1	1	-1769	5310	13	-18.3
0	2	-2197	0	-13.2	0
1	2	3074	-2356	3.7	-15
2	2	1685	-425	-.6	-6.0
0	3	1320	0	1.5	0
1	3	-2268	-261	-6.4	4.1
2	3	1246	302	-.2	2.2
3	3	766	-406	-8.1	-12.1
0	4	941	0	.8	0
1	4	782	262	.9	1.8
2	4	291	-232	-6.9	1.2
3	4	-421	99	.5	2.7
4	4	116	-301	-4.6	-1
0	5	-210	0	.8	0
1	5	352	44	.1	.2
2	5	237	157	-1.5	1.2
3	5	-122	-152	-2	.3
4	5	-167	-64	-.1	1.8
5	5	-26	99	2.3	.9
etc.					

REPORT DOCUMENTATION PAGE

Form Approved
OMB No. 0704-0188

1. AGENCY USE ONLY *(Leave blank)*	2. REPORT DATE	3. REPORT TYPE AND DATES COVERED
	October 1999	Technical Memorandum

4. TITLE AND SUBTITLE
The Geomagnetic Field and Radiation in Near-Earth Orbits

5. FUNDING NUMBERS
920

6. AUTHOR(S)
J.R. Heirtzler

7. PERFORMING ORGANIZATION NAME(S) AND ADDRESS (ES)
Earth Sciences Directorate
Laboratory for Terrestrial Physics
Goddard Space Flight Center
Greenbelt, Maryland 20771

8. PEFORMING ORGANIZATION REPORT NUMBER
99B00083

9. SPONSORING / MONITORING AGENCY NAME(S) AND ADDRESS (ES)
National Aeronautics and Space Administration
Washington, DC 20546-0001

10. SPONSORING / MONITORING AGENCY REPORT NUMBER
TM—1999–209481

11. SUPPLEMENTARY NOTES

12a. DISTRIBUTION / AVAILABILITY STATEMENT
Unclassified–Unlimited
Subject Category: 46
Report available from the NASA Center for AeroSpace Information,
7121 Standard Drive, Hanover, MD 21076-1320. (301) 621-0390.

12b. DISTRIBUTION CODE

13. ABSTRACT *(Maximum 200 words)*

This report shows, in detail, how the geomagnetic field interacts with the particle flux of the radiation belts to create a hazard to spacecraft and humans in near-Earth orbit. It illustrates the geometry of the geomagnetic field lines, especially around the area where the field strength is anomalously low in the South Atlantic Ocean. It discusses how the field will probably change in the future and the consequences that may have on hazards in near space.

14. SUBJECT TERMS
Geomagnetic field; particle flux; radiation belt; near-Earth orbit; radiation hazards in near space.

15. NUMBER OF PAGES
36

16. PRICE CODE

17. SECURITY CLASSIFICATION OF REPORT	18. SECURITY CLASSIFICATION OF THIS PAGE	19. SECURITY CLASSIFICATION OF ABSTRACT	20. LIMITATION OF ABSTRACT
Unclassified	Unclassified	Unclassified	UL